analytical chemistry

Article

pubs.acs.org/ac

Exploring Metabolic Pathways in Vivo by a Combined Approach of Mixed Stable Isotope-Labeled Raman Microspectroscopy and Multivariate Curve Resolution Analysis

Hemanth Noothalapati[†] and Shinsuke Shigeto*[,†]

[†]Department of Applied Chemistry and Institute of Molecular Science, National Chiao Tung University, Hsinchu 30010, Taiwan

Supporting Information

ABSTRACT: Understanding cellular metabolism is a major challenge in current systems biology and has triggered extensive metabolomics research, which in most cases involves destructive analysis. However, the information obtainable only in a nondestructive manner will be required for accurately mapping the global structure of the organism's metabolic network at a given instant. Here we report that metabolic pathways can be explored in vivo by mixed stable isotope-labeled Raman microspectroscopy in conjunction with multivariate curve resolution analysis. As a model system, we studied ergosterol biosynthesis in single living fission yeast cells grown in mixtures of normal and ^{13}C-labeled glucose as the sole carbon source. The multivariate spectral data analysis of space-resolved Raman spectra revealed the intrinsic spectra and relative abundances of all isotopomers of ergosterol whose carbon atoms in the 5,7-diene moiety of the sterol skeleton are either partly or fully substituted with ^{13}C. Our approach is applicable to other metabolites and will earn a place in the toolbox of metabolomic analysis.

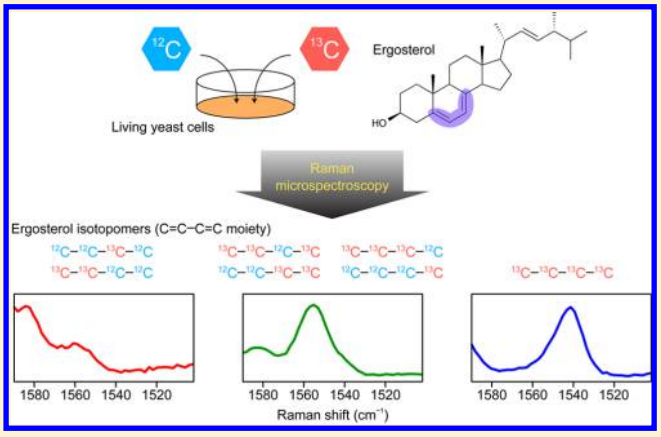

The postgenomic era of biology aims to understand the interaction and connectivity of higher levels of organization in the cell and eventually to delineate a detailed picture of the whole organism at a given instant.[1−3] At the heart of this grand design is cellular metabolism, the exceedingly complex web of enzymatic chemical reactions from which all living organisms derive energy for their survival and growth. Elucidation of the metabolic network is not only of fundamental importance but it also provides valuable strategies for metabolic engineering directed toward efficient materials production through genetic manipulation.

Most current knowledge on metabolic pathways has been gained from biochemical analysis using isotope tracers. Isotope labeling introduces asymmetry in the dimension of time, thus facilitating the tracing of metabolic processes. Traditionally, radioactive isotopes were used, but because of health risks and inherent difficulties in handling and storage, radioisotopes have been replaced by their stable counterparts. Pioneering work with the use of stable isotopes in biological research was conducted as early as in the 1930s by Schoenheimer and Rittenberg[4] and Cavanagh and Raper,[5] who investigated incorporation of deuterium-labeled fatty acids into fat tissues in mice. Recent technological advances in nuclear magnetic resonance and mass spectrometry have ushered in a myriad of powerful, stable isotope-based methods in the emerging field of metabolomics, such as metabolic flux analysis (MFA),[6,7] mass isotopomer distribution analysis (MIDA),[8] stable isotope labeling by amino acids in cell culture (SILAC),[9−12] DNA-based stable-isotope probing (DNA-SIP),[13,14] and RNA-based SIP.[15,16] Nevertheless, it remains an open question how individual metabolic fluxes are dynamically interconnected and globally organized so as to fulfill their mission in the metabolic network, primarily because the aforementioned methods require destructive procedures and/or lack space specificity.

Raman microspectroscopy, being endowed with nondestructiveness and subcellular resolution,[17−24] is complementary to the conventional biochemical and mass spectrometry approaches and hence holds promise to address the question by studying metabolic pathways and relevant phenomena in vivo. The method is fully compatible with the stable isotope labeling strategy. The frequency of a vibrational mode observed with Raman spectroscopy is inversely proportional to the square root of the reduced mass of the mode. Thus, when light atom(s) involved in the molecular vibration are substituted with heavier isotopes, the vibrational frequency will be reduced and the corresponding Raman band will red-shift, making it possible to identify and discriminate isotopically substituted molecular species. SIP coupled with Raman spectroscopy has been used to reveal long-term extracellular activity of

Received: May 9, 2014
Accepted: June 29, 2014
Published: June 30, 2014

dx.doi.org/10.1021/ac501735c | Anal. Chem. 2014, 86, 7828−7834

chlamydiae,[25] carbon dioxide fixation by single cells,[26] and carbon flow in a food chain.[27] Recently we applied ^{13}C-labeled Raman imaging, where ^{13}C-glucose was used as the sole carbon source, to the model eukaryote fission yeast (*Schizosaccharomyces pombe*), and visualized for the first time dynamic proteome localization to lipid droplets at the single-cell level.[28]

In this paper, we employ light (^{12}C) and heavy (^{13}C) carbon isotope mixtures to study metabolic pathways in living cells. Using ^{12}C/^{13}C mixtures with the total carbon content kept constant is essential because the relative abundances of multiply ^{13}C-substituted isotopomers of a metabolite are anticipated to change systematically, depending on its metabolic pathway. The more different carbon atoms in the metabolite are substituted with ^{13}C, and the more intermediate Raman bands appear between fully ^{12}C and ^{13}C bands. Analysis of those "molecular fingerprints" enables us to identify all possible isotopomers. By varying the ^{13}C content available to *S. pombe* cells, we investigated ergosterol anabolism without resort to extraction and isolation of intracellular components of relevance. Global spectral data analysis using multivariate curve resolution (MCR) yielded the intrinsic spectra of different ^{13}C isotopomers of ergosterol that have ^{13}C isotope substitution in the conjugated C=C bond (i.e., 5,7-diene) moiety of the sterol skeleton, as well as the isotopomer distributions. These are entirely new results that were unobtainable previously.[28] We discuss the feasibility of our combined approach of mixed stable isotope-labeled Raman microspectroscopy and MCR as an effective analytical tool for exploring metabolic pathways in vivo.

EXPERIMENTAL SECTION

Cell Culture. Wild-type *Schizosaccharomyces pombe* was used in this study. *S. pombe* cells were precultured on yeast extract with supplements (YES), containing yeast extract (5 g L^{-1}), glucose (30 g L^{-1}), adenine, histidine, leucine, uracil, and lysine hydrochloride (225 mg L^{-1} each). A single colony of precultured *S. pombe* cells was inoculated into a 3 mL portion of Edinburgh minimal medium (EMM), containing D-glucose (20 g L^{-1}), potassium hydrogen phthalate (3 g L^{-1}), NH_4Cl (5 g L^{-1}), and Na_2HPO_4 (2.2 g L^{-1}), salts, vitamins, and minerals. In EMM, glucose was the sole carbon source available to *S. pombe* cells. Mixtures of normal ^{12}C-glucose and uniformly labeled ^{13}C-glucose (99 atom % ^{13}C; Cambridge Isotope Laboratories) with ^{13}C contents of 0, 10, 20, 25, 30, 40, 50, 60, 70, 75, 80, 90, and 100% were used. Note that for simplicity, the ^{13}C content discussed throughout this paper does not take into account natural abundance of ^{13}C (~1.1%), which makes no essential difference in our analysis. Cells were incubated in EMM broth at 30 °C under shaking conditions for 2 days. A 2 μL portion of this culture was sandwiched between two glass coverslips and used for Raman measurements without any further sample pretreatment.

Confocal Raman Microspectroscopy. All Raman measurements were performed with a laboratory-built confocal Raman microspectrometer (see Figure S1 in the Supporting Information for a schematic of the apparatus), which has been described in detail elsewhere.[23,29] Briefly, the 632.8 nm output of a He−Ne laser was used as the Raman excitation source. The laser beam was introduced to an inverted microscope (Nikon, customized TE2000) and focused onto the sample with an oil immersion objective (100×, NA = 1.3). Backscattered light collected by the same objective traveled through the edge filter to remove Rayleigh scattering (and anti-Stokes scattering) and then through a 100 μm pinhole to achieve confocal detection. Stokes Raman light was dispersed by an imaging spectrometer (HORIBA Scientific, iHR320) and detected by a back-illuminated, liquid N_2-cooled CCD detector (Princeton Instruments, Spec-10:100). The laser power at the sample was 2.7 mW, and exposure time per cell was 60 s. Under these conditions, no significant photodamage on the cell was found. The spectral resolution of our Raman microspectrometer was about 6 cm^{-1}. The lateral and axial resolution achieved was 0.3 and 3 μm, respectively. All measurements were done at room temperature (23 °C).

Density Functional Theory (DFT) Calculations. DFT calculations on all 16 isotopomers of the ergosterol molecule in the gas phase were performed at the B3LYP/6-31+G(2d,p) level of theory using Gaussian 09.[30] Geometry optimization was followed by harmonic frequency calculations. The lack of anharmonicity in the calculated B3LYP spectra was partially compensated by performing a uniform scaling of the computed frequencies by a factor of 0.965.

Multivariate Analysis. In MCR, a low-rank approximation of the matrix $\mathbf{M}$ (an $m \times n$ non-negative data matrix) is obtained by solving the following equation:

$$\mathbf{M} = \mathbf{WH} \tag{1}$$

with all elements of matrices $\mathbf{W}$ (an $m \times k$ matrix) and $\mathbf{H}$ (a $k \times n$ matrix) being restricted to be non-negative.[31,32] Because of the non-negativity constraints, MCR tends to yield sparse, physically interpretable solutions and is thus more amenable to spectral analysis than other multivariate methods such as principal component analysis (PCA) and singular value decomposition (SVD). The optimal solution of $\mathbf{W}$ and $\mathbf{H}$ is determined by solving alternating least-squares (ALS) problems[31] of eq 1 so that the norm $\| \mathbf{M} - \mathbf{WH} \|$ is minimized. In the present study, the parameter k, which denotes the number of underlying components, was set to be $k = 3$ (three-component model).

Prior to MCR analysis, a constant offset that was chosen to be the minimum count in the spectral region of interest was subtracted from each raw spectrum. A total of 325 offset-corrected spectra (25 spectra from 13 media), each of which consisted of 46 pixels (1502−1590 cm^{-1}), were consolidated to generate the data matrix $\mathbf{M}$ (a 46 × 325 matrix). SVD-based initialization[33] was used to obtain initial guesses for $\mathbf{W}$ and $\mathbf{H}$. ALS optimization of $\mathbf{W}$ and $\mathbf{H}$ with L1-norm regularization (also known as lasso regression[34]) was then carried out until satisfactory convergence was achieved. During 4000 times iteration, an L1 penalty term of $\alpha^2 = 0.005$ was added to obtain sparser solutions as

$$(\mathbf{W}^T\mathbf{W} + \alpha^2\mathbf{E})\mathbf{H} = \mathbf{W}^T\mathbf{M} \tag{2}$$

$$(\mathbf{H}\mathbf{H}^T + \alpha^2\mathbf{E})\mathbf{W} = \mathbf{H}\mathbf{M}^T \tag{3}$$

where $\mathbf{E}$ is a $k \times k$ matrix all of whose elements are unity. The MCR was performed on a software (nmf-11, Pylone) developed specifically for Raman applications.[29]

To confirm the validity of the MCR, another well-established multivariate method, agglomerative hierarchical cluster analysis (AHCA),[35] was also carried out on the same Raman data set. Euclidean distance measure was used to calculate the distance matrix. Ward's algorithm was used to merge individual spectra of high similarity into clusters and construct the dendrogram of the Raman spectra. AHCA was performed employing the hyperspec package in R (version 3.0.3).[36]

dx.doi.org/10.1021/ac501735c | Anal. Chem. 2014, 86, 7828−7834

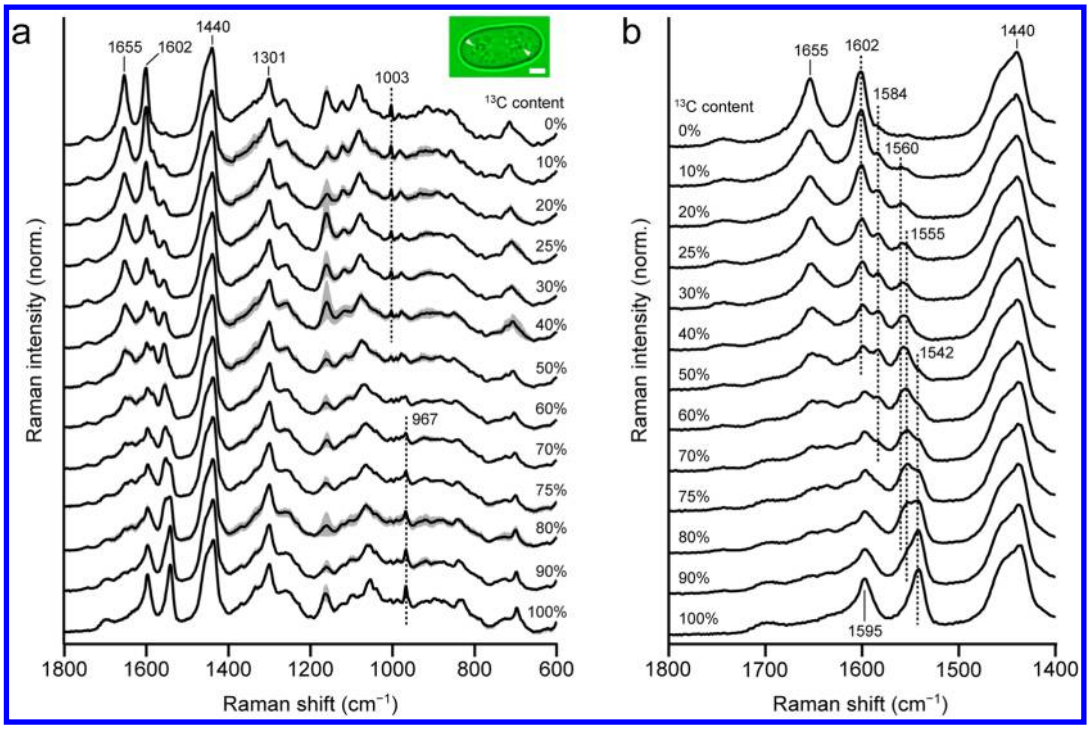

Figure 1. Space-resolved Raman spectra of living *S. pombe* cells cultured in mixed isotope media. (a) The whole fingerprint region (600−1800 cm^{-1}). The shaded area represents the 1σ error envelope. All of the averaged spectra have been normalized to the area of the CH bending band at 1440 cm^{-1}. The inset shows an optical image of a typical *S. pombe* cell, where a couple of lipid droplets are indicated by arrowhead. Scale bar = 2 μm. (b) Enlarged view of the 1400−1800 cm^{-1} region, which was analyzed in detail.

RESULTS AND DISCUSSION

Raman Spectra of *S. pombe* Grown in Mixtures of ^{12}C- and ^{13}C-Glucose. To probe carbon flow during metabolic pathways in vivo, we measured a sequence of space-resolved Raman spectra of lipid droplets in living *S. pombe* cells cultured for 2 days in EMM containing mixtures of ^{12}C- and uniformly labeled ^{13}C-glucose as the sole carbon source at different ^{13}C concentrations (Figure 1). To suppress uncertainties arising from cell individuality, we obtained Raman spectra from 25 randomly selected *S. pombe* cells in each isotope mixture, and the average of 25 spectra is shown in Figure 1. The Raman spectra were collected exclusively from lipid droplets (see the inset of Figure 1a), because they are known to be the organelle that gives rise to a very intense Raman band of ergosterol,[37] which is the primary interest in this study.

The overall spectral change in the so-called fingerprint region with increasing ^{13}C content from 0 (pure ^{12}C EMM) to 100% (pure ^{13}C EMM) can be seen in Figure 1a, revealing several pronounced ^{13}C isotope substitution effects. The *cis*-C═C stretching mode of lipids shifts from 1655 to 1595 cm^{-1}. Similarly, the ring-breathing mode of phenylalanine residues of proteins, which appears as a sharp, characteristic peak at 1003 cm^{-1} in pure ^{12}C EMM, shifts to 967 cm^{-1} in media with ^{13}C content higher than 70%. In contrast, the bands at 1440 and 1301 cm^{-1} assigned respectively to the CH bending and in-plane CH_2 twisting modes do not show noticeable peak shift upon ^{13}C isotope substitution. These observations agree very well with our and other previous reports.[25,28,38] Although the lipid C═C stretching and phenylalanine ring-breathing bands show gradual ^{13}C shifts depending on the ^{13}C content in the medium, it is prohibitively difficult to attribute those bands to specific lipid/protein molecules and look into their biosynthetic pathways. Thus, we focus here on the behavior of the Raman band that appears at 1602 cm^{-1} in 100% ^{12}C medium; this band arises predominantly from the C═C−C═C symmetric stretch of the 5,7-diene structure in ergosterol[37] (vide infra).

In Figure 1b, which is an enlarged view of the spectral region 1400−1800 cm^{-1}, we anticipate to see the Raman bands of ergosterol isotopomers. A couple of new bands at ∼1584 and ∼1560 cm^{-1} are clearly discernible even at as low as 10% of ^{13}C in the medium. As ^{13}C content is increased to 30%, the 1584 cm^{-1} band becomes more prominent and the 1560 cm^{-1} band appears to get broadened. This apparent broadening is due to the emergence of an additional peak at ∼1555 cm^{-1} as a shoulder of the 1560 cm^{-1} band. At 60% ^{13}C content, the bands at 1584, 1560, and 1555 cm^{-1} start to disappear slowly, whereas a new peak is identified at around 1542 cm^{-1}, which in the end grows to be the strongest band with further increasing ^{13}C content. This band does not appear clearly even as a shoulder until ^{13}C content reaches 60%. As already assigned in our previous study,[28] this band undoubtedly originates from the ergosterol isotopomer in which all four carbon atoms involved in the 5,7-diene structure are substituted with ^{13}C (see Figure 3 for the chemical structure of ergosterol). Because there is no prominent Raman band, except for the C═C stretching band of lipids (red-shifted to 1595 cm^{-1}), that could come into the spectral window between 1500 and 1600 cm^{-1} upon ^{13}C isotope substitution, we can safely argue that the Raman features discussed above are all attributed to different ergosterol isotopomers. The intermediate bands at 1584, 1560, and 1555 cm^{-1} have not been observed before[28] and must be attributed to the ergosterol molecules whose carbon atoms in the diene moiety are partially (1, 2, or 3 carbon atoms) substituted with ^{13}C.

Resolving the Isotopomers with Multivariate Curve Resolution Analysis. In this work, we used MCR[39−42] to

dx.doi.org/10.1021/ac501735c | *Anal. Chem.* 2014, 86, 7828−7834

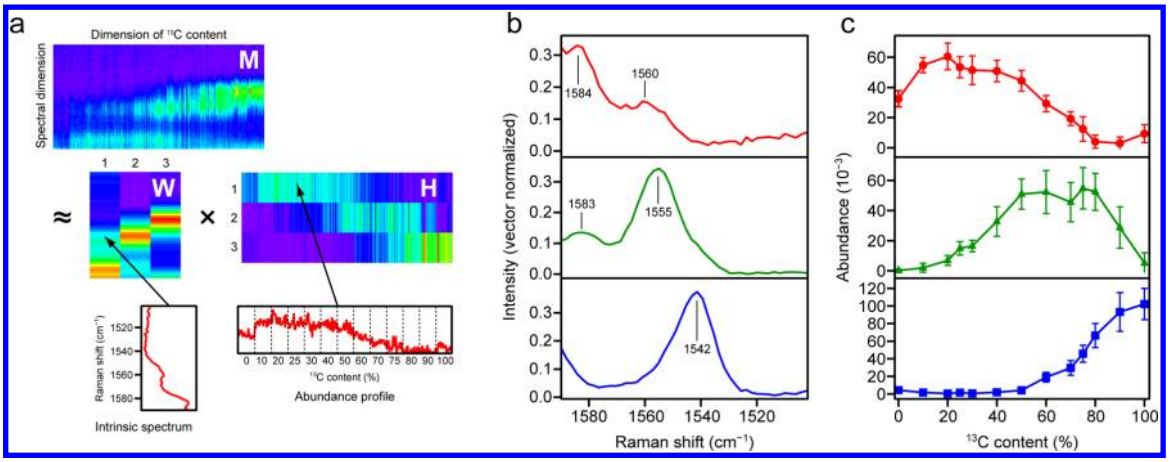

Figure 2. (a) Schematic illustration of the principle of MCR assuming three components. The data matrix **M** subjected to MCR was a 46 × 325 matrix that consisted of 25 Raman spectra at 13 different ^{13}C contents. Columns of the matrix **W** represent the intrinsic spectra of the resolved components shown in b, whereas rows of the matrix **H** represent their abundance profiles. Every 25 points in each row of **H** correspond to the relative abundances of the component in 25 different *S. pombe* cells at respective ^{13}C contents, which are averaged to obtain the relative abundance profiles shown in c. (b and c) Intrinsic spectra (b) and ^{13}C content dependences of relative abundance (c) of the three components. Data in c represent mean values ± standard deviations (n = 25).

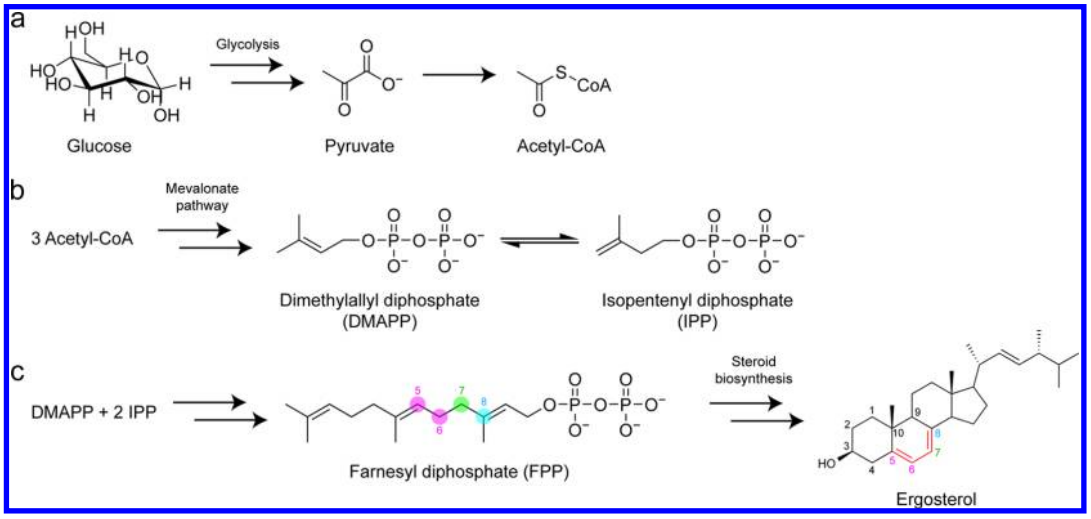

Figure 3. Important steps to track carbon flow during ergosterol biosynthesis in yeast. (a) Conversion of glucose to pyruvate via glycolysis followed by its decarboxylation, forming acetyl-CoA. (b) Initial steps in the mevalonate pathway, where acetyl-CoA is converted to form DMAPP and its isomer IPP. (c) Formation of FPP and conversion of FPP to ergosterol via steroid biosynthesis. The four carbon atoms C5−C8 in the 5,7-diene moiety of the ergosterol molecule and corresponding atoms in FPP are highlighted by red, green, and blue to indicate that the C5 and C6 atoms (red) are of the same isotope, but the C7 (green) and C8 (blue) atoms can have different isotopic characters.

derive more quantitative information on the partially ^{13}C-substituted ergosterol species from the severely congested spectra shown in Figure 1. MCR has found many applications in data mining and pattern recognition, but we have recently demonstrated that it is applicable to Raman microspectroscopy and imaging as well.[29] As illustrated in Figure 2a, MCR approximates matrix **M**, which in the present case consists of a total of 325 spectra at 13 different ^{13}C contents, as the product of two low-rank, non-negative matrices **W** and **H**. The matrices **W** and **H** represent the intrinsic spectra and ^{13}C content dependences of relative abundance (abundance profiles) of resolved components, respectively. Here only a narrow region between 1502 and 1590 cm^{-1} of the data shown in Figure 1 was used in constructing the matrix **M**, because inclusion of Raman bands other than those of ergosterol might complicate MCR analysis. Furthermore, the 1602 cm^{-1} band (in 100% ^{12}C medium) was excluded to reduce the influence of overlap of the red-shifted C═C stretching band at 1595 cm^{-1}. Such careful choice of the spectral window to be analyzed enhances the reliability of MCR.

MCR assuming three components successfully disentangles the intrinsic spectra (Figure 2b) and relative abundance profiles (Figure 2c). Such clear resolution would not be successful if one applies ordinary curve fitting to decompose the complex spectra. The number of components in MCR is completely arbitrary and needs to be input a priori by the user. We attempted MCR analysis assuming two and four components, but the former resulted in insufficient decomposition and the latter in the appearance of redundant components. To further check the validity of the present MCR analysis with three components, we calculated the residual matrix. A two-dimensional plot of the residual matrix (Figure S2b, Supporting Information) shows no particular distribution pattern, and the residues appear to be uniformly distributed. Furthermore,

dx.doi.org/10.1021/ac501735c | Anal. Chem. 2014, 86, 7828−7834

typical preprocessed spectra and the corresponding MCR fitted spectra look quite similar (Figure S2c–f, Supporting Information). Together, we confirm that the original data are well reproduced by the three components. The three-component model can also be justified by biochemical consideration, as discussed below.

The first component shows two bands peaking at ∼1560 and 1584 cm^{-1} (Figure 2b, red line). As evident from the relative abundance profile (Figure 2c, red line), this component is dominant at low ^{13}C contents (<60%), indicating that mono-^{13}C-substituted (and perhaps disubstituted) ergosterol isotopomers contribute to the first component. In the spectrum of the second component (Figure 2b, green line), two peaks are found at Raman shifts similar to those of the first component, i.e., 1555 and 1583 cm^{-1}. On the other hand, the relative abundance profile is substantially different (Figure 2c, green line): it monotonically increases up to 50% ^{13}C, plateaus between 50% and 80%, and then declines over 80%. This dependence suggests that the second component is mainly due to di- and trisubstituted isotopomers. It is straightforward to assign the third component to the fully ^{13}C-substituted species because the spectrum (Figure 2b, blue line) contains a sole band at 1542 cm^{-1}, in agreement with what we observe in the averaged spectrum in pure ^{13}C EMM (Figure 1b). The monotonically increasing abundance profile over the entire range of ^{13}C content (Figure 2c, blue line) is also consistent with this assignment.

Carbon Flow during Ergosterol Biosynthesis in Yeast. So far we have determined the spectral features and relative abundances of the three groups of ergosterol isotopomers in a quantitative manner. To identify each member of those groups, we need to know (1) how glucose is utilized in ergosterol biosynthesis, (2) the number of all possible isotopomers of ergosterol, (3) vibrational frequencies of each isotopomer, and (4) dependence on ^{13}C content of the abundance of each isotopomer. These tasks can be performed by tracking carbon flow during the ergosterol biosynthetic pathways in yeasts and performing quantum chemical calculations on possible isotopomers.

Important reactions in ergosterol biosynthesis[43] pertinent to the discussion here are summarized in Figure 3. First, glucose incorporated in the cell is converted in a series of steps to pyruvate via glycolysis. Pyruvate is then decarboxylated to form acetyl-CoA (Figure 3a), which plays a major role in carbohydrate and fatty acid metabolisms. Acetyl-CoA enters the mevalonate pathway, where dimethylallyl diphosphate (DMAPP) and its isomer isopentenyl diphosphate (IPP) are produced (Figure 3b). Next, in two consecutive steps, one molecule of DMAPP and two molecules of IPP are combined to form farnesyl diphosphate (FPP) as shown in Figure 3c. A four-carbon skeleton (labeled C5–C8 in Figure 3c, according to the carbon atom numbering in the ergosterol molecule), which leads to the diene structure of ergosterol, is created at this stage. Once FPP is formed, the four-carbon skeleton is preserved until FPP is eventually converted to ergosterol via subsequent steroid synthesis. The most important point here is that the 5,7-diene structure of ergosterol is constructed from three different acetyl-CoA molecules and that the C5 and C6 atoms come from the same acetyl-CoA. It follows from this fact that these carbon atoms must be of the same isotope irrespective of ^{13}C content in the medium, whereas the C7 and C8 atoms can have different isotopic characters. Therefore, although 16 (= 2^4) different isotopomers are theoretically conceivable, only 8 (= 2^3) of them are practically permissible. The isotope combinations in the eight isotopomers are shown in Table 1.

Table 1. Summary of Calculated and Experimental Vibrational Frequencies of the Eight Possible Ergosterol Isotopomers 1–8 (a uniform scaling factor of 0.965 was used)

	Isotope combination in 5,7-diene (C5–C6–C7–C8)	DFT calculated frequency (cm^{-1})	Experimental frequency (cm^{-1})	Expected ^{13}C content (x) dependence
1	^{12}C–^{12}C–^{12}C–^{12}C	1602.0	1602	—
2	^{12}C–^{12}C–^{12}C–^{13}C	1581.1	∼1584	$x(1-x)^2$
3	^{12}C–^{12}C–^{13}C–^{12}C	1579.1		
4	^{13}C–^{13}C–^{12}C–^{12}C	1565.9	∼1560	
5	^{13}C–^{13}C–^{12}C–^{13}C	1558.5	∼1555–1560	$x^2(1-x)$
6	^{13}C–^{13}C–^{13}C–^{12}C	1556.8		
7	^{12}C–^{12}C–^{13}C–^{13}C	1553.7		
8	^{13}C–^{13}C–^{13}C–^{13}C	1540	1542	x^3

Next we performed DFT calculations to predict the vibrational frequency of each of the eight possible isotopomers (denoted 1–8), and results are shown in Table 1. The calculated ^{13}C isotope shift (62 cm^{-1}) is in excellent agreement with the experimental value (60 cm^{-1}). Similar calculations were also performed on the remaining eight isotopomers that are not permissible according to the biosynthetic pathways, and calculated frequencies are listed in Table S1, Supporting Information. Those isotopomers are predicted to appear in the 1585–1590 cm^{-1} region and at ∼1570 cm^{-1}, where experimentally no noticeable band is observed in any isotope mixture whatsoever (Figure 2b).

Assuming statistical distribution of ^{13}C isotope in the 5,7-diene moiety, isotopomers 2–4 (two mono- and one disubstituted species) should show the ^{13}C content dependence of $x(1-x)^2$, where x is the fractional ^{13}C content ($0 \le x \le 1$). Recall that the C5 and C6 atoms must always have the same isotopic character and is considered as a single entity. Isotopomers 5–7 (one di- and two trisubstituted species) constitute another group that shows the dependence of $x^2(1-x)$. Finally, isotopomer 8 (the fully substituted species) should exhibit a cubic dependence on ^{13}C content. The classification of the seven isotopomers 2–8 into three groups justifies the three-component model employed in the MCR analysis.

Assignment of MCR-Derived Ergosterol Isotopomers. With the biochemical knowledge on ergosterol biosynthesis and DFT calculation results in mind, we now discuss in depth the three components derived from the MCR analysis (Figure 2b,c). It is clear that the first MCR component represents the group of isotopomers 2–4. In the intrinsic spectrum (Figure 2b, red line), the band at ∼1584 cm^{-1} is most likely associated with isotopomers 2 and/or 3 and that at ∼1560 cm^{-1} with isotopomer 4. Also, the relative abundance profile (Figure 2c, red line) is well explained by the expected dependence ($x(1-x)^2$) in terms of the overall shape and an approximate location of the maximum (theory predicts it to be 33%). The nonzero abundance at $x = 0$ may be due to considerable overlap with the unsubstituted ergosterol band at 1602 cm^{-1}. Likewise, we

dx.doi.org/10.1021/ac501735c | Anal. Chem. 2014, 86, 7828–7834

attribute the second MCR component to the group of isotopomers 5−7. These isotopomers are so close to each other in vibrational frequency that they cannot be resolved experimentally. In other words, they may underlie the intense Raman band at 1560 cm^{-1} (Figure 2b, green line). Agreement between the experimentally derived abundance profile (Figure 2c, green line) and the predicted dependence $(x^2(1 - x))$ is remarkably good. As a matter of fact, the third MCR component corresponds to isotopomer 8, the fully substituted species. In this way, we have shown that the intrinsic spectra and relative abundance profiles derived from the MCR analysis of mixed stable isotope-labeled Raman data enable us to track the ergosterol biosynthetic pathways in vivo and in a quantitative manner.

Comparison with Hierarchical Cluster Analysis. Although our interpretation accounts almost perfectly for the MCR results, the origin of the band at 1583 cm^{-1} in the second MCR component (Figure 2b, green line) remains unclear. None of isotopomers 5−7 is predicted by DFT to appear at around this Raman shift. It may be argued that the appearance of the band at ∼1584 cm^{-1} in both spectra of the first and second MCR components is simply due to imperfect separation of components in the present MCR analysis. To examine whether this feature is specific to MCR or not, we compare the MCR results (Figure 2) with those obtained by a different type of multivariate method, AHCA (Figure 4). AHCA is widely

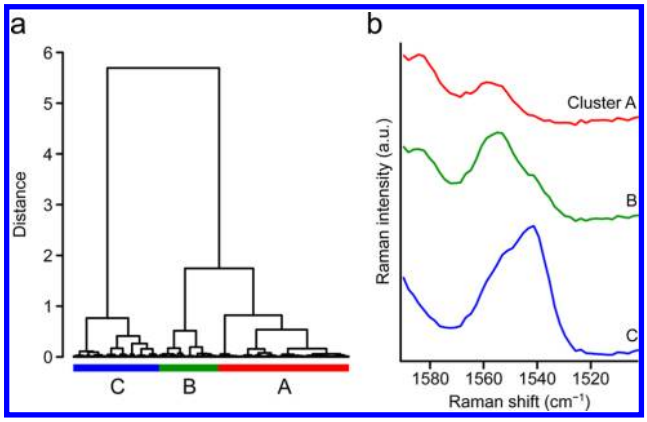

Figure 4. AHCA of the same Raman data set as used for the MCR analysis. (a) Dendrogram of the Raman spectra, showing a clear segmentation of the data into three clusters A−C. (b) Mean cluster Raman spectra of the three clusters. Each mean spectrum was calculated by averaging all of the Raman spectra that belong to the respective cluster.

used for Raman hyperspectral data analysis. By way of example, El-Mashtoly et al.[44] recently reported that HCA can visualize several cellular components in colon cancer cells that are not well separated by other multivariate methods including MCR and PCA.

The dendrogram (Figure 4a) indicates that the observed Raman spectra can be classified into three clusters of high similarity (denoted A−C). This result is consistent with the three-component model deployed in the MCR analysis. The mean cluster Raman spectra of the three clusters (Figure 4b) are quite analogous in pattern as well as band peaks to the intrinsic spectra derived from the MCR (Figure 2b), corroborating the MCR results. The most notable difference between the two outputs is that the mean spectrum of cluster C from AHCA (Figure 4b, blue line) has a clear shoulder at the higher-wavenumber side of the 1542 cm^{-1} peak, whereas the spectrum of the third MCR component (Figure 2b, blue line) displays a single band. We also looked into four and five clusters from AHCA, but the resulting mean cluster spectra did not vary much as compared with those shown in Figure 4b, save for minor differences in baseline shape. From the above comparison, it is less likely that the 1583 cm^{-1} band observed for the second MCR component results solely from insufficient resolution of different isotopomers. Further clarification of the origin of this band is left for future studies.

CONCLUSIONS

We have demonstrated the unique ability of mixed stable isotope ($^{12}C/^{13}C$) labeled Raman microspectroscopy in combination with MCR to study metabolic pathways in vivo. Extension of this work to imaging and dynamics studies would be an attractive direction to go. Until the recent report by Chiu et al.,[37] the origin of the 1602 cm^{-1} Raman band was unclear. In the present study, we have further reinforced (almost concluded) the assignment of this band to the conjugated C═C stretching mode of ergosterol. Raman spectroscopic approaches using this ergosterol marker band could have important implications for online monitoring of ethanol production in industry[45,46] and for routine fungal biomass monitoring.[47,48] Although this paper has focused on analysis of ergosterol in *S. pombe*, our method should be applicable to other metabolites in different organisms (e.g., animal cells and plant cells), and in tandem with biochemical and mass spectrometry-based approaches, it could be useful for unraveling yet unknown metabolic processes in living cells.

ASSOCIATED CONTENT

Supporting Information

Additional information as noted in text. This material is available free of charge via the Internet at http://pubs.acs.org.

AUTHOR INFORMATION

Corresponding Author

*E-mail: shigeto@mail.nctu.edu.tw.

Notes

The authors declare no competing financial interest.

ACKNOWLEDGMENTS

This work was supported in part by the ATU plan of the Ministry of Education, Taiwan, by National Chiao Tung University, and by the Ministry of Science and Technology of Taiwan (grant no. NSC102-2113-M-009-012 to S.S.).

REFERENCES

(1) Stelling, J.; Klamt, S.; Bettenbrock, K.; Schuster, S.; Gilles, E. D. *Nature* **2002**, *420*, 190−193.
(2) Hellerstein, M. K. *Annu. Rev. Nutr.* **2003**, *23*, 379−402.
(3) Almaas, E.; Kovács, B.; Vicsek, T.; Oltvai, Z. N.; Barabási, A.-L. *Nature* **2004**, *427*, 839−843.
(4) Schoenheimer, R.; Rittenberg, D. *Science* **1935**, *82*, 156−157.
(5) Cavanagh, B.; Raper, H. S. *Nature* **1936**, *137*, 233−234.
(6) Fischer, E.; Sauer, U. *Nat. Genet.* **2005**, *37*, 636−640.
(7) Niklas, J.; Schneider, K.; Heinzle, E. *Curr. Opin. Biotechnol.* **2010**, *21*, 63−69.
(8) Hellerstein, M. K.; Neese, R. A. *Am. J. Physiol.* **1992**, *263*, E998−1001.

(9) Ong, S.-E.; Blagoev, B.; Kratchmarova, I.; Krishtensen, D. B.; Steen, H.; Pandey, A.; Mann, M. *Mol. Cell. Proteomics* **2002**, *1*, 376−386.
(10) Ong, S.-E.; Mann, M. *Nat. Protoc.* **2006**, *1*, 2650−2660.
(11) Bendall, S. C.; Hughes, C.; Stewart, M. H.; Doble, B.; Bhatia, M.; Lajoie, G. A. *Mol. Cell. Proteomics* **2008**, *7*, 1587−1597.
(12) Doherty, M. K.; Hammond, D. E.; Clague, M. J.; Gaskell, S. J.; Beynon, R. J. *J. Proteome Res.* **2009**, *8*, 104−112.
(13) Radajewski, S.; Ineson, P.; Parekh, N. R.; Murrell, J. C. *Nature* **2000**, *403*, 646−649.
(14) Uhlík, O.; Jecná, K.; Leigh, M. B.; Macková, M.; Macek, T. *Sci. Total Environ.* **2009**, *407*, 3611−3619.
(15) Manefield, M.; Whiteley, A. S.; Griffiths, R. I.; Bailey, M. J. *Appl. Environ. Microbiol.* **2002**, *68*, 5367−5373.
(16) Whiteley, A. S.; Manefield, M.; Lueders, T. *Curr. Opin. Biotechnol.* **2006**, *17*, 67−71.
(17) Puppels, G. J.; de Mul, F. F. M.; Otto, C.; Greve, J.; Robert-Nicoud, M.; Arndt-Jovin, D. J.; Jovin, T. M. *Nature* **1990**, *347*, 301−303.
(18) Uzunbajakava, N.; Lenferink, A.; Kraan, Y.; Volokhina, E.; Vrensen, G.; Greve, J.; Otto, C. *Biophys. J.* **2003**, *84*, 3968−3981.
(19) Xie, C.; Li, Y.-q. *J. Appl. Phys.* **2003**, *93*, 2982−2986.
(20) Singh, G. P.; Volpe, G.; Creely, C. M.; Grötsch, H.; Geli, I. M.; Petrov, D. *J. Raman Spectrosc.* **2006**, *37*, 858−864.
(21) Moritz, T. J.; Taylor, D. S.; Polage, C. R.; Krol, D. M.; Lane, S. M.; Chan, J. W. *Anal. Chem.* **2010**, *82*, 2703−2710.
(22) Huang, C.-K.; Hamaguchi, H.; Shigeto, S. *Chem. Commun.* **2011**, *47*, 9423−9425.
(23) Noothalapati Venkata, H. N.; Nomura, N.; Shigeto, S. *J. Raman Spectrosc.* **2011**, *42*, 1913−1915.
(24) Palonpon, A. F.; Sodeoka, M.; Fujita, K. *Curr. Opin. Chem. Biol.* **2013**, *17*, 708−715.
(25) Haider, S.; Wagner, M.; Shmid, M. C.; Sixt, B. S.; Christian, J. G.; Häcker, G.; Pichler, P.; Mechtler, K.; Müller, A.; Baranyi, C.; Toenshoff, E. R.; Montanaro, J.; Horn, M. *Mol. Microbiol.* **2010**, *77*, 687−700.
(26) Li, M.; Canniffe, D. P.; Jackson, P. J.; Davison, P. A.; FitzGerald, S.; Dickman, M. J.; Burgess, J. G.; Hunter, C. N.; Huang, W. *ISME J.* **2012**, *6*, 875−885.
(27) Li, M.; Huang, W. E.; Gibson, C. M.; Fowler, P. W.; Jousset, A. *Anal. Chem.* **2013**, *85*, 1642−1649.
(28) Noothalapati Venkata, H. N.; Shigeto, S. *Chem. Biol.* **2012**, *19*, 1373−1380.
(29) Huang, C.-K.; Ando, M.; Hamaguchi, H.; Shigeto, S. *Anal. Chem.* **2012**, *84*, 5661−5668.
(30) Frisch, M. J.; et al. *Gaussian 09, Revision D.01*; Gaussian, Inc., Wallingford, CT, 2009.
(31) Paatero, P.; Tapper, U. *Environmetrics* **1994**, *5*, 111−126.
(32) Lee, D. D.; Seung, H. S. *Nature* **1999**, *401*, 788−791.
(33) Boutsidis, C.; Gallopoulos, E. *Pattern Recognit.* **2008**, *41*, 1350−1362.
(34) Tibshirani, R. *J. R. Statist. Soc. B* **2011**, *73*, 273−282.
(35) Miljković, M.; Chernenko, T.; Romeo, M. J.; Bird, B.; Matthäus, C.; Diem, M. *Analyst* **2010**, *135*, 2002−2013.
(36) Beleites, C.; Sergo, V. R package version 0.98-20140220. http://hyperspec.r-forge.r-project.org.
(37) Chiu, L.-d.; Hullin-Matsuda, F.; Kobayashi, T.; Torii, H.; Hamaguchi, H. *J. Biophotonics* **2012**, *5*, 724−728.
(38) Huang, W. E.; Stoecker, K.; Griffiths, R.; Newbold, L.; Daims, H.; Whiteley, A. S.; Wagner, M. *Environ. Microbiol.* **2007**, *9*, 1878−1889.
(39) Andrew, J. J.; Hancewicz, T. M. *Appl. Spectrosc.* **1998**, *52*, 797−807.
(40) de Juan, A.; Tauler, R. *Anal. Chim. Acta* **2003**, *500*, 195−210.
(41) Shafer-Peltier, K. E.; Haka, A. S.; Motz, J. T.; Fitzmaurice, M.; Dasari, R. R.; Feld, M. S. *J. Cell. Biochem. Suppl.* **2002**, *39*, 125−137.
(42) Shinzawa, H.; Awa, K.; Kanematsu, W.; Ozaki, Y. *J. Raman Spectrosc.* **2009**, *40*, 1720−1725.
(43) Parks, L. W.; Casey, W. M. *Annu. Rev. Microbiol.* **1995**, *49*, 95−116.
(44) El-Mashtoly, S. F.; Petersen, D.; Yosef, H. K.; Mosig, A.; Reinacher-Schick, A.; Kötting, C.; Gerwert, K. *Analyst* **2014**, *139*, 1155−1161.
(45) Zaldivar, J.; Nielsen, J.; Olsson, L. *Appl. Microbiol. Biotechnol.* **2001**, *56*, 17−34.
(46) Sun, Y.; Cheng, J. *Bioresour. Technol.* **2002**, *83*, 1−11.
(47) Gardner, R. M.; Tindall, G. W.; Cline, S. M.; Brown, K. L. *J. Microbiol. Methods* **1993**, *17*, 49−60.
(48) Mille-Lindblom, C.; von Wachenfeldt, E.; Tranvik, L. J. *J. Microbiol. Methods* **2004**, *59*, 253−262.